Electronic Supplementary Information (ESI) for "Optical-signal-enhancing metasurface platforms for fluorescent molecules at water-transparent near-infrared wavelengths"

H. Kurosawa and M. Iwanaga*
National Institute for Materials Science, 1-1 Namiki, Tsukuba 305-0044, Japan
*E-mail: iwanaga.masanobu@nims.go.jp

S1 Stacked Complementary Structure

Figure S1 shows typical section-view SEM images of a Au stacked complementary (SC) plasmo-photonic (PlasPh) metasurface [1]: (a) top-view SEM images and (b) a section-view SEM image. Figure S1a has a white scale bar indicating 1 μm; the inset is a magnified view. The top-view image visualizes Au in the top layer of the SC PlasPh metasurface and air holes.

Figure S1b shows a section-view of the SC structure; the section corresponds to a *xz* section in Fig. 2a. The white parts represent Au, indicated by white arrows and forming the top and bottom layers. The middle layer is perforated silicon-on-insulator (SOI) layer. White scale bar indicates 200 nm. Thus, we confirmed that the design for the SC metasurface is realized as intended.

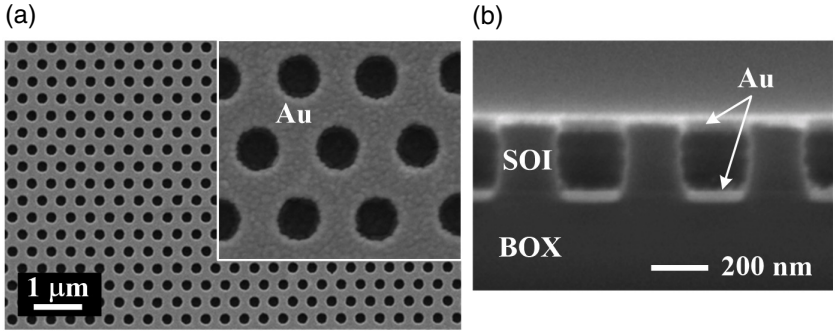

Figure S1: Structural confirmation of Au SC PlasPh metasurfaces. (a) Typical top-view SEM images. White scale bar indicates 1 μm. The inset is a magnified image. (b) Section-view of SEM image. White arrows indicates Au in the top and bottom layers. The deposited metal was Au and the thickness was set to 35 nm. The positions of SOI and buried oxide (BOX) are also shown. White scale bar indicates 200 nm. These images were adapted from [1].

S2 Additional Optical Spectra

Figure S2 shows measured reflectance (R) spectra of Au SC PlasPh metasurfaces. Three cases are shown: air-hole diameter (D) 212, 220, and 280 nm. They indirectly appeared in Fig. 2 and 3 through eqn (1) in the text.

These R spectra were directly measured using a spectrometer equipped with incident-angle resolved system. The incident angle was 5°, close to the normal incidence, and the incident polarization was

set to p polarization, being parallel to the plane of incidence. The PlasPh metasurfaces were set in the spectrometer such that the horizontal axis is x axis in Fig. 2a and the vertical axis is y axis.

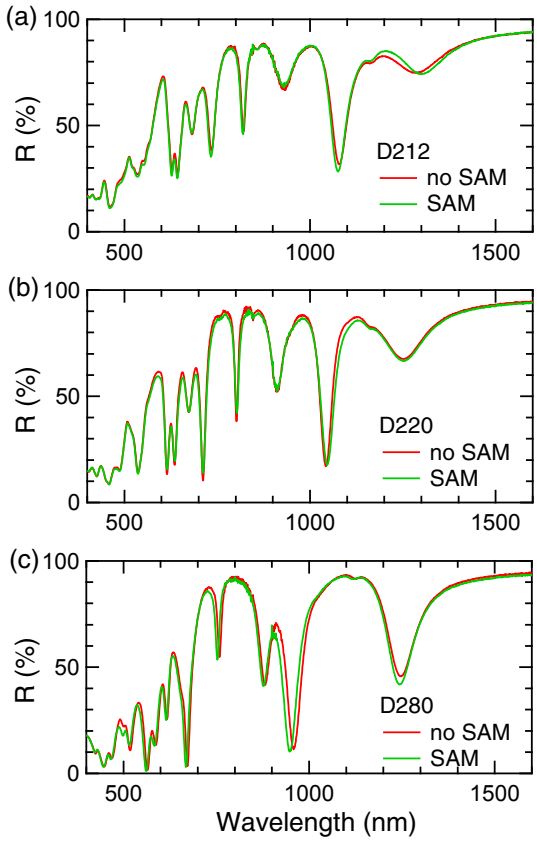

Figure S2: Measured reflectance (R) spectra of Au SC PlasPh metasurfaces. (a) Air hole diameter (D) 212 nm. (b) D 220 nm. (c) D 280 nm. Red and green lines denote SC PlasPh metasurface without and with SAM of 15-CPDT, respectively. The deposited metal was Au and the thickness was set to 35 nm.

The air-hole diameters contribute to resonant wavelengths, in particular, to the second resonance corresponding to deep R dips at 1080, 1030, and 950 nm in Fig. S2a, b and c, respectively. The property is consistent with the results in a previous paper [2].

Figure S2 also shows difference with and without self-assembled monolayer (SAM). The R spectra of the PlasPh metasurfaces without SAM are shown with red lines and those with SAM of 15-carboxy-1-pentadecanethiol (15-CPDT) are shown with green lines. Note that the 15-CPDT is described in the text (see Fig. 3). It is evident that the SAM hardly affects the R spectra. We believe that slight difference of the R spectra mostly comes from fluctuations in Au deposition. The PlasPh metasurfaces with and without SAM were prepared in different Au-deposition lots though the base nanoimprinted SOI substrates were in common through the present study.

Figure S3 shows the enhanced optical signal in Fig. 2c with wavenumber representation. Sharp 11 peaks at 428, 486, 527, 578, 749, 1044, 1092, 1164, 1237, 1393 and 1565 cm^{-1} are indicted by vertical short bars. being attributable to Raman signals of IR26 molecules, which are consistent with a previous report [3].

Figure S4 shows measured R spectra of Ag SC PlasPh metasurfaces without any SAM: (a) air-hole diameter D 212 nm, (b) D 223 nm and (c) D 280 nm. The diameters are almost the same as those in Fig. S2 since the base nanoimprinted SOI substrates are in common. The slight difference in the diameters comes from metallic grains grown in the deposition process. As the diameters become larger, the second resonance that is deep reflectance dip around 1000 nm shifts to shorter wavelengths. This

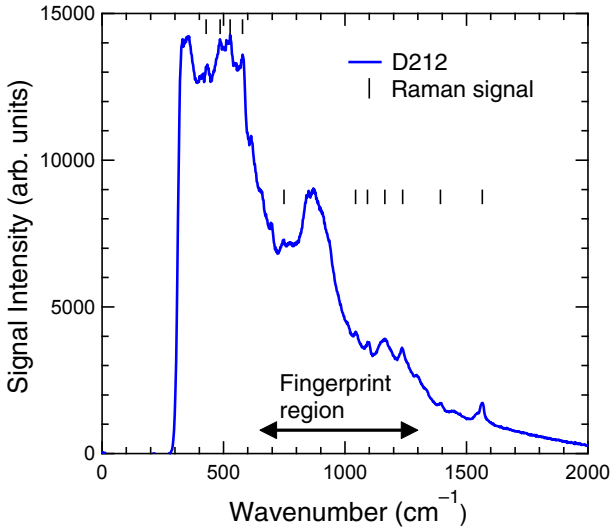

Figure S3: Measured optical signal represented with wavenumber. 11 vertical short bars indicate the Raman signals. This spectrum is in common with Fig. 2c. Both-end arrow indicates molecular fingerprint region from 650 to 1300 cm^{-1}.

tendency is similar to the Au SC PlasPh metasurfaces. The resonant wavelengths are also quite close in the equivalent diameter metasurfaces. Thus, Au and Ag result in similar reflectance spectra in the SC PlasPh metasurfaces.

Figure S5 shows results of optical measurement on an IR26-molecule-dispersed SiO_2 substrate. The setup and preparation were the same as those described in section 4.1 in the text. Therefore, the data in Fig. S5 are comparable to the fluorescence spectrum in Fig. 1c. Obviously, the signal intensities from the SiO_2 substrate are much smaller than the intensity from the Si wafer; in fact, it is difficult to extract definite signals from Fig. S5, since the signal-to-noise ratio is less than 1. This means that it is practically impossible to use the data for evaluating the enhancement factors listed in Table 1. Thus, we adopted the Si wafer as the reference substrate. We also conducted similar measurement on flat Au film and found that the film is unsuitable for the reference owing to the extremely small signals (or virtually no signal).

S3 Further Numerical Data

Figure S6 shows a set of numerical results for a Ag SC PlasPh metasurface that has the same structural parameters to the Au metasurface in Fig. 5 and 6. In the computations, Au was simply replaced with Ag. We present these results to confirm the similar resonant features in Ag and Au PlasPh metasurfaces.

Figure S6a shows light absorptance spectrum of the Ag PlasPh metasurface at the normal incidence that is linearly x-polarized in the optical configuration (Fig. 2a). The incidence was set to travel from the air side and to illuminate the top layer of perforated Ag film. The absorptance was evaluated using calculated reflectance and eqn (1) in the text. The numbers 1 and 2 indicate the first and second resonances, respectively; note that the order is defined in photon energies, inversely proportional to wavelengths. When comparing this absorptance spectrum with that in Fig. 5a, it is obvious that the two spectra are very similar to each other both qualitatively and quantitatively. This result is consistent with the measured data on reflectance spectra, which are similar in the Ag and Au cases as shown in Fig. S2 and S4.

Figure S6b shows electric-field intensity $|\mathbf{E}|^2$ at the second resonance in an xz section, which is taken in the same manner to Fig. 6. Thus, Figure S6b is directly comparable to Fig. 6b. Figure S6b is displayed in the logarithmic scale and a saturated manner similar to Fig. 6; this presentation is in common with Fig. 6. We note that the maximum value in Fig. S6b is 1632, being about 9% larger than that in the Au case (1498). Overall, we can conclude that the $|\mathbf{E}|^2$ distributions are qualitatively very similar in the Ag and

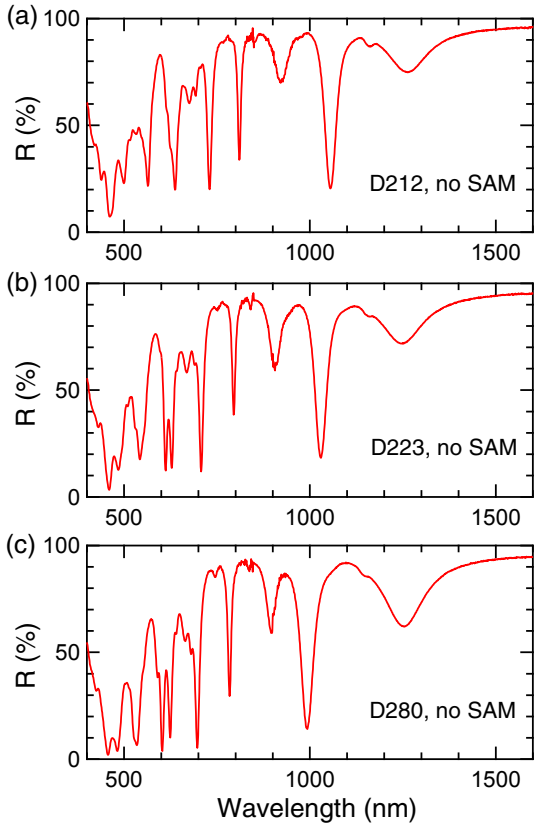

Figure S4: Measured R spectra of Ag SC PlasPh metasurfaces (red lines). (a) Air hole diameter (D) 212 nm. (b) D 223 nm. (c) D 280 nm. The deposited metal was Ag. The thickness was set to 35 nm.

Au cases.

Figure S6c and d shows absolute values of electric fields $|\mathbf{E}|$ at the second resonance in xy sections; each z position is indicated by a white dashed line in Fig. S6b. Figure S6c and d corresponds to the surfaces of the top and bottom layers in the SC structure, respectively. Also, the linear scale is commonly shown at the bottom and the $(0, 5)$ range is identical to that in Fig. 5b. Evidently, the distributions in Fig. S6 are quite similar to those in Fig. 5b.

Thus, the resonant electric-field distributions strongly suggest that, if we assume that the enhancement effects for optical signals from the dispersed IR26 molecules come from the electric-field enhancement, the Ag and Au cases result in similar enhancement effects and that the Ag case is expected to be relatively better. However, our observations do not support this simple assumption. Therefore, we discuss the origin of the enhancement effects in more deeper manner in section 2.2.

Figure S7 shows complex relative permittivity of the noble metals: (a) Au and (b) Ag. Measured and cited data are shown. The measured data were obtained by ellipsometry using the deposited noble-metal thin films on quartz substrates. For comparison, complex relative permittivity from literature [4] is shown with black. In both cases, the real and imaginary parts are displayed with solid and dashed curves, respectively. The imaginary parts are quite close in the values while the real parts exhibit quantitative difference. The measured permittivities take more negative values than those in the literature, which results in the difference in resonant wavelengths. When we used the measured permittivities, the resonances corresponding to the peaks of absorptance appear at shorter wavelengths, typically by 40 nm, and show better reproduction of the measured data. Therefore, we used measured permittivities in the computations.

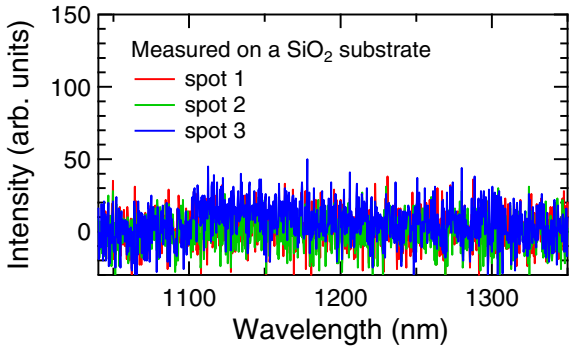

Figure S5: Test measurement for a SiO_2 substrate to examine the suitability for reference. The present data are comparable to the fluorescence spectrum in Fig. 1c. The IR26 molecules were dispersed in an equivalent way to the Si wafer. Three colored lines indicate three measurement results at different light-illumination spots. The setup and measurement conditions were the same as those described in section 4.1 and 4.2.

References

[1] B. Choi, M. Iwanaga, H. T. Miyazaki, K. Sakoda and Y. Sugimoto, *J. Micro/Nanolithogr. MEMS MOEMS*, 2014, **13**, 023007.

[2] M. Iwanaga, B. Choi, H. T. Miyazaki, Y. Sugimoto and K. Sakoda, *J. Nanomater.*, 2015, **2015**, 507656.

[3] Y. Nishijima, Y. Hashimoto, L. Rosa, J. B. Khurgin and S. Juodkazis, *Appl. Phys. A*, 2014, **117**, 647–650.

[4] A. D. Rakić, A. B. Djurušić, J. M. Elazar and M. L. Majewski, *Appl. Opt.*, 1998, **37**, 5271–5283.

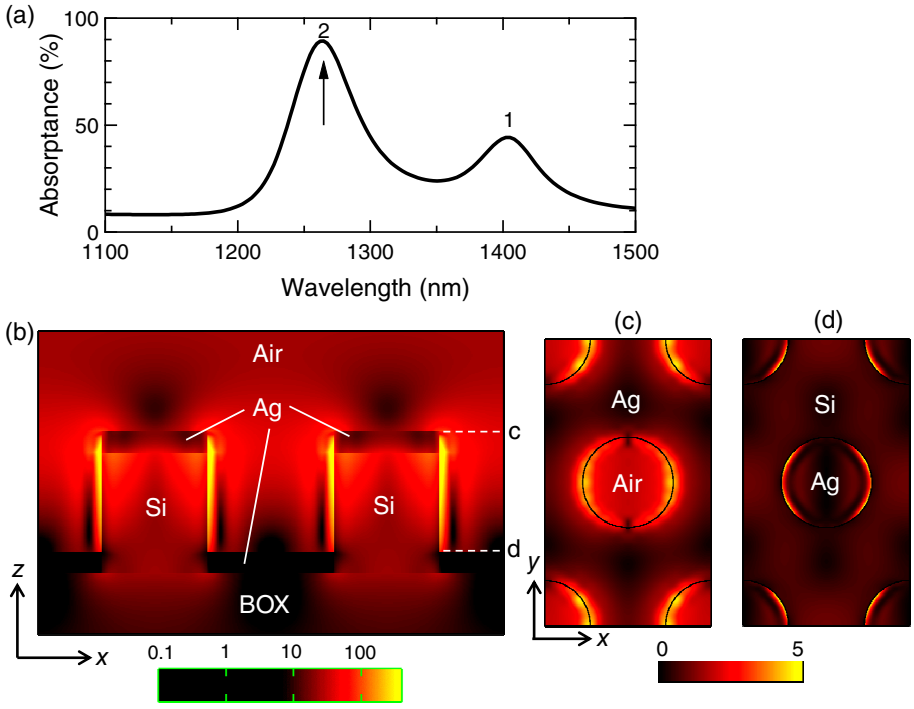

Figure S6: Resonances in a Ag PlasPh metasurface. (a) Light absorptance spectra. (b) Electric-field intensity $|\mathbf{E}|^2$ at the second resonance in a *xz* section, which was taken in the same way to Fig. 6. The $|\mathbf{E}|^2$ distribution is plotted in the logarithmic scale and presented in a saturated manner that set the maximum $|\mathbf{E}|^2$ to be 400. This presentation is the same to Fig. 6. (c) and (d) Absolute values of electric fields $|\mathbf{E}|$ at the second resonance in *xy* sections; the *z* positions are indicated by white dashed lines in (b). These *xy* sections were taken in the same way to Fig. 5b.

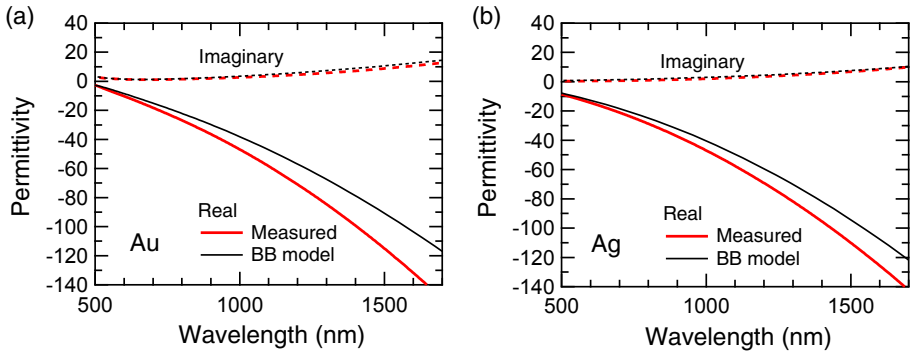

Figure S7: Complex relative permittivity. (a) Au. (b) Ag. Measured data are shown with red. The literature values [4] are shown with black. The real and imaginary parts are shown with solid and dashed curves, respectively.